Volume 1 | Number 1 | Jan 2013 | Pages 1–100

Dalton Transactions

An international journal of inorganic chemistry
www.rsc.org/dalton

ROYAL SOCIETY OF CHEMISTRY

This is an *Accepted Manuscript*, which has been through the Royal Society of Chemistry peer review process and has been accepted for publication.

Accepted Manuscripts are published online shortly after acceptance, before technical editing, formatting and proof reading. Using this free service, authors can make their results available to the community, in citable form, before we publish the edited article. We will replace this *Accepted Manuscript* with the edited and formatted *Advance Article* as soon as it is available.

You can find more information about *Accepted Manuscripts* in the **Information for Authors**.

Please note that technical editing may introduce minor changes to the text and/or graphics, which may alter content. The journal's standard **Terms & Conditions** and the **Ethical guidelines** still apply. In no event shall the Royal Society of Chemistry be held responsible for any errors or omissions in this *Accepted Manuscript* or any consequences arising from the use of any information it contains.

www.rsc.org/dalton

Dalton Transactions

ARTICLE

New Pd(II) Hemichelates Devoid of Incipient Bridging CO…Pd interactions[†]

Christophe Werlé,[a] Dylan M. Anstine,[a,b] Lydia Karmazin,[a] Corinne Bailly,[a] Louis Ricard[c] and Jean-Pierre Djukic[*,a]

In organometallic chemistry the commonly known Sidgwick-Langmuir 18 electron rule is constantly being probed for further discovery of molecular compounds that arise as exceptions. The present study examines the formation and the structure of three novel hemichelates of Pd(II) derived from the reaction of in situ-formed indene and hydrophenanthrene-based organometallic anions with three different μ-chloro-bridged palladacycles. Electronic structure and interaction behavior have been calculated with methods of the Density Functional Theory at the (ZORA) MetaGGA-D TPSS-D3(BJ), GGA-D PBE-D3(BJ), and hybrid PBE0-dDsC dispersion corrected levels, all with the implementation of all electron triple zeta single polarization basis set. A particular focus of the theoretical investigation was made on the nature of the interaction between the $[Cr(CO)_3]$ moiety and the Pd(II) centers, which according to X-ray diffraction analyses lack of significant incipient bridging CO…Pd character. Structures were further assessed with Natural Bonding Orbitals (NBO), Quantum Theory of Atoms in Molecules (QTAIM), and Extended Transition State with Natural Orbitals for Chemical Valence (ETS-NOCV) analysis methods. As a result, intramolecular interactions of interest, primarily around the Pd atom, were analyzed as a measure of natural atomic orbital (NAO) contributions to the natural bonding orbital (NBO) formation, QTAIM analysis with special attention to the bonding critical points (BCPs), as well as energetic analysis of intramolecular interaction forces by Energy Decomposition Analysis (EDA). Theoretical analyses confirm that attractive electrostatics dominate the stabilization of Pd(II) hemichelates. In the case of complexes **1c**, **2c** and **3c** we expand the known amount of 14 electron transition metal complexes that can be synthesized via reliable synthetic methods. However, complex **3c** presented some means of stability but was more reactive to moisture and air in laboratory conditions and escaped thorough analytical characterization.

Introduction

The Sidgwick-Langmuir 18 electron rule[1] is a general scheme for the stability of complexes involving a transition metal center.[1, 2] A significant amount of exceptions to the Sidgwick-Langmuir 18 electron rule manifest themselves in various ways that still fuel sustained fundamental research on the pertinence[3-9] of this empirical extension of the so-called octet rule.[10-12] The current introduction of the concept of hemichelation[13-15] has opened up the doors for transition metal complexes to be observed in a manner in which forces beyond the covalent interactions are significantly contributing to the stability of their apparently 18-electron rule infringing structures.[16] Loosely defined,

hemichelation[13-15] is the particular way in which ligands interact with a transition metal via one coordinative interaction and one non-covalent interaction. The interest in this particular mode of stabilization can be attributed to the observed persistent and air/moisture stable complexes that contain electron deficient centers.[13-15, 17-22] The stability of the presented complexes results in some non-conventional coordination modes of transition metal complexes. Experimental and computational data are presented to describe the structure of these molecules with special attention to the noncovalent contributions to stability. More important, it is proposed therein that the weak incipient Cr-CO…Pd interaction of donor-acceptor (dative) character[15, 21] observed in previous experimental

Journal Name

ARTICLE

structures of Pd complexes is not central to the stabilisation of the formally electron-deficient Pd(II) centres.

Results and discussion

Previous reports have demonstrated the validity of the concept of hemichelation in that a large series of formally 14 electron electron unsaturated Pd(II),[13, 21] Pd(I),[15] Pt(II)[13], Rh(I)[14], and 16 electron Mn(I)[18-20] and Re(I)[18-20] complexes containing various ligand retinues could be synthesized in a chemically stable form. In the case of Pd and Pt complexes, a rather important number of X-ray diffraction analyses indicated the existence of incipient CO-M interactions with C-M distances matching the expectation for a semibridging CO situation,[23-29] a widely documented interaction often encountered in electron unsaturated polymetalcarbonyl complexes that is believed to substantially contribute to molecular cohesion.[30, 31]

Figure 1. The syntheses of **1c**-**3c**.

In our previous reports, Extended Transition State-Natural Orbitals for Chemical Valence (ETS-NOCV)[32, 33] analyses indicated in most investigated cases that such incipient interaction had a donor-acceptor character allowing electron density transfer from the $Cr(CO)_3$ moiety towards the M center. It was also shown that this $[Cr(CO)_3] \rightarrow Pd$ interaction was compensated by $Pd \rightarrow Cr$ back donation through the ligand, therefore relativising the weight of such dative bond in the overall interaction scheme implying direct $[Cr(CO)_3]$-Pd interactions of covalent and non-covalent nature. Taking into consideration the *in solutio* behaviour of Pd and Pt hemichelates we further argued that such weak dative interaction was certainly unimportant to the molecular cohesion because the $Cr(CO)_3$ moiety could still rotate causing the periodic disruption/construction of the $[Cr(CO)_3] \rightarrow Pd$ interaction. In the crystal state, the $Cr(CO)_3$ rotor is static and the observed structures displaying the Cr-CO…Pd interaction can be considered as minima of energy within the context of crystal-state whereby the crystal lattice is known to operate great influence over local and intramolecular geometries.[34] Quite interestingly, in our previous studies dealing with Pd(II and I)[13, 15, 21] and Pt(II)[13] hemichelates, most gas-phase optimized geometries reproduced this incipient semi-bridging CO situation, which was characterized by a marked covalent through in the NCI regions plots.[35, 36] In contrast, none of the reported Rh(I) hemichelates displayed such an incipient semi-bridging CO situation. The quest for cases of Pd(II) hemichelates where such interaction would not be encountered in the crystal state was therefore initiated. Our synthetic effort led to three new complexes **1c**-**3c** (Figure 1) synthesized from 2-methylindene and di-hydroanthracene derivatives, i.e. **1a**-**3a**, by the sequential deprotonation of the benzylic position and the trapping of the organolithium intermediate by different palladacycles, i.e. (*R*)-**1b**, **2b**, **3b**. It is worthy to note that **2a** consisted of a mixture of the homo- and hetero-chiral (meso) diastereomers, of which only the hetero-chiral one afforded a stable product, i.e **2c** (17 % yield based on the add mixture of homo- and hetero-chiral **2a**).

With the exception of **3c**, which escaped thorough analytical investigations due to unexpected high reactivity, the other hemichelate and double hemichelate **1c** and **2c** respectively where found stable and rather persistent in solution in aprotic solvents. Both **1c** and **2c** displayed IR features consistent with the powder-ATR-FT-IR spectra reported for similar hemichelates of palladacycles.[13] The IR signature was characterized by three bands at ca. 1930, 1865 and 1840 cm^{-1} that were assigned, according to DFT calculations, to one symmetric (*A*) and two asymmetric stretching modes for the CO ligands of the $Cr(CO)_3$ moieties. Solution ^{13}C NMR spectra of **1c** and **2c** at room temperature indicated three distinct broad resonances (239.5, 237.3 and
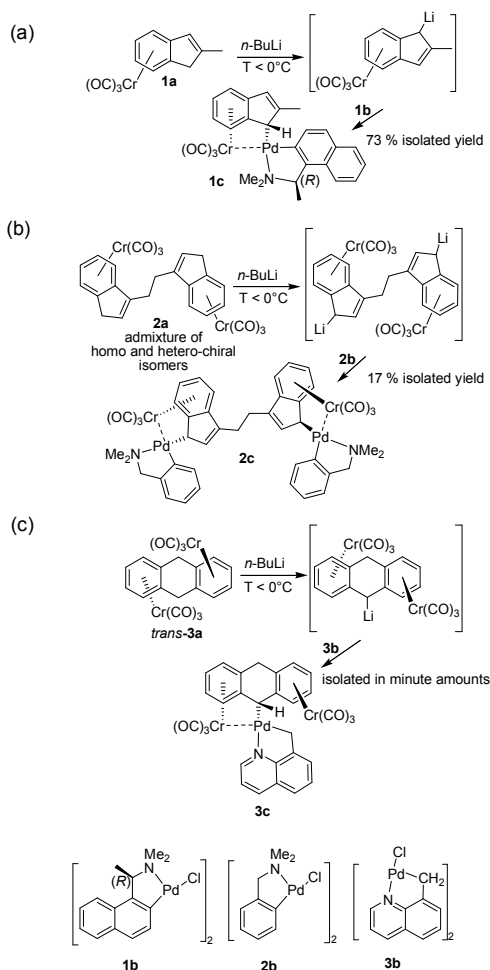
Dalton Transactions

ARTICLE

235.2 ppm for **1c** and 238.7, 236.4 and 232.7 ppm for **2c** originating from the $Cr(CO)_3$ moiety, which within the time scale of the ^{13}C NMR (125 MHz) can be interpreted like a symptom of slowed rotation of the latter rotor.[17]
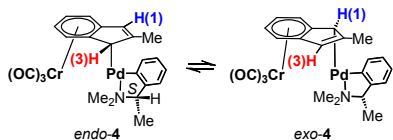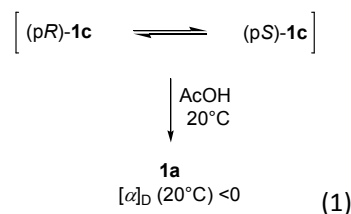

Figure 2. In solution, complex **4** displayed a dynamic behavior consisting of a fast migration of the palladacyclic unit.[13]

The ^{1}H NMR spectra of **1c** and **2c** did not reveal obvious signs of possible "palladotropism", that is the fast 1-3 migration of the palladacyclic unit from one benzylic position at C1 to its equivalent at C3. This observation is consistent with observations made for similar hemichelates of palladacycles. Owing to the low value of the barrier of activation of such palladotropism, i.e $\Delta G^{\neq}$ (298 K) <10 kcal/mol,[13, 21] ^{1}H NMR (600 MHz) spectroscopy was unable to sense the dynamic exchange within **1c** even at low temperatures. Compound **1c** did not crystallize as a 1:1 mixture of two diastereomers, like compound **4** (Figure 2),[13] but as a single diastereomer of absolute (p*R*,1*R*) configuration ($[\alpha]_D$ (298 K)= -267.3) in a non-centrosymmetric space group (vide infra, Figure 3, Table 4). Upon protonation of **1c** with acetic acid at 20°C (eq 1), planar chiral **1a** was recovered in scalemic (non-racemic) form with a specific rotation $[\alpha]_D$(20°C) of -11.5 expressing a slight predominance of (p*R*)-**1a** (*ee* < 10) according to previous results[13] obtained for the protonation of **4**. This suggests that at room temperature in solution **1c** exists as a fast exchanging non-equimolar mixture of two diastereomers, namely (p*S*,1*R*)-**1c** and (p*R*,1*R*)-**1c**. Furthermore, TD-DFT simulation of the gas-phase CD spectrum of (p*S*,1*R*)-**1c** using the *statistical average of orbital model exchange-correlation* potential (ZORA-SAOP[37, 38]/all electron TZ2P), produced an excellent match to the experimental CD spectrum recorded in benzene at 20°C (cf. ESI), which displays two characteristic Cotton effects at around 480 (positive) and 400 (negative) nm. This suggests that (p*S*,1*R*)-**1c** might be the dominating diastereomer in solution. The situation of **2c** is different for the two benzylic positions are inequivalent; the steric strain produced by the bridging ethylenyl substituent that occupies one benzylic position at each indenyl fragments may indeed prevent palladotropism.

$$\left[(pR)\text{-}\mathbf{1c} \rightleftharpoons (pS)\text{-}\mathbf{1c} \right]$$

$$\downarrow \begin{array}{c} AcOH \\ 20°C \end{array}$$

$$\begin{array}{c} \mathbf{1a} \\ [\alpha]_D \ (20°C) <0 \end{array} \qquad (1)$$

Structural characterization of 1c-3c

Expectedly, in the three structures displayed in Figure 3 the $Cr(CO)_3$ tripod is anti-eclipsed with respect to the benzylic position that bears the palladacyclic unit. By comparison to previously reported structures of Pd(II) and Pd(I) hemichelates[13, 15, 21] the distance separating carbonyl carbon atoms from Pd (cf Pd-CO, Table 1) is by 0.15-0.20 Å longer in **1c-3c**. This geometrical feature is consistent with the Cr-Pd distances that span 2.92-2.88 Å like observed in previously reported Pd(II) hemichelates containing palladacycles.[13]
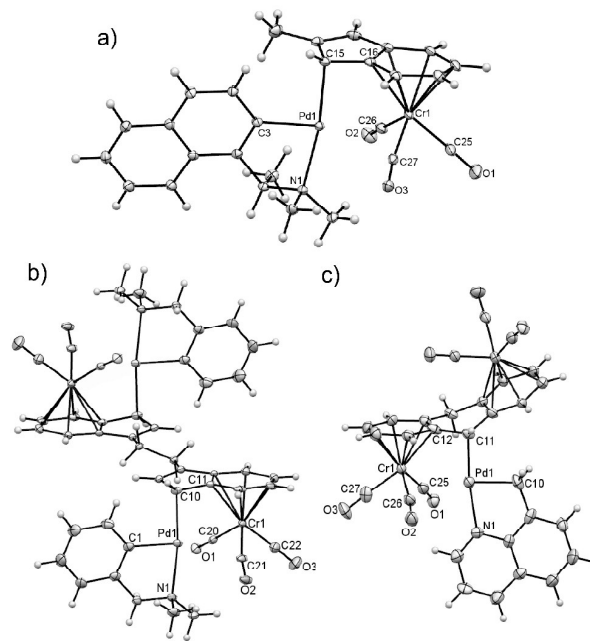

Figure 3. ORTEP-type drawings of the structures of (p*S, 1R*)-**1c** (a), **2c** (b) and **3c** (c) with partial atom numbering. Ellipsoids are drawn at the 30 % probability level. Selected interatomic angles for **1c** (deg): C15-Pd1-C3 90.63(11), C3-Pd1-N1 79.85(10), C26-Cr1-C27 99.68(13), C15-Pd1-N1 170.46(10). Selected interatomic angles for **2c** (deg): C10-Pd1-N1 171.90(8), C10-Pd1-C1 90.51(9), C20-Cr1-C21 98.05(10), C10-Pd1-N1 171.90(8). Selected interatomic angles for **3c** (deg): C11-Pd1-C10 88.7(4), C11-Pd1-N1 170.1(3), C26-Cr-C25 97.7(5), C10-Pd1-N1 82.3(4). See Table 1 for selected distances.

Theoretical analysis of hemichelates 1c-3c

Geometry optimization. Molecular geometries were optimized at three separate levels of theory; TPSS-D3(BJ),

Journal Name

ARTICLE

PBE-D3(BJ), and PBE0-dDsC, using the Amsterdam Density Functional (ADF) software package.[39, 40] As denoted, dispersion-corrected functionals were used to address the diffuse and non-local attractive interactions that occur in large transition metal complexes.[41-43] To convey the accuracy of the geometry optimization, distances between the palladium center and surrounding atoms at the three levels of theory are listed in Table 1. The atomic distances are all within 0.06 Å of one another.

Table 1: Distances (in Å) between particular atoms in complexes **1c-3c** in X-ray diffraction structures and in models computed at various levels of theory. All distances are listed in Å.

1c	atom num.[a]	exptl	PBE-D3(BJ)[b]	TPSS-D3(BJ)[b]	PBE0-dDsC[b]
Cr-Pd	Cr1-Pd1	2.9294(5)	2.909	2.841	2.833
Pd–C$_{benz}$	Pd1-C15	2.117(3)	2.142	2.142	2.124
Pd-C	Pd1-C3	2.017(2)	2.033	2.041	2.014
Pd-N	Pd1-N1	2.170(2)	2.196	2.176	2.172
Pd-CO	Pd1-C26/C27	2.70/2.74	2.62/2.62	2.59/2.72	2.55/2.68
2c					
Cr-Pd	Cr1-Pd1	2.8925(4)	2.845	2.786	
Pd–C$_{benz}$	Pd1-C10	2.111(2)	2.141	2.138	
Pd-C	Pd1-C1	2.020(2)	2.037	2.038	
Pd-N	Pd1-N1	2.1915(18)	2.207	2.190	
Pd-CO	Pd1-C20/C21	2.65/2.65	2.55/2.67	2.62/2.49	
3c					
Cr-Pd	Cr1-Pd1	2.8874(16)	2.813	2.785	2.812
Pd-C$_{benz}$	Pd1-C11	2.057(9)	2.124	2.121	2.085
Pd–C	Pd1-C10	2.034(9)	2.072	2.073	2.037
Pd-N	Pd1-N1	2.111(8)	2.128	2.115	2.114
Pd-CO	Pd1-C25/C26	2.65/2.75	2.49/2.62	2.50/2.60	2.47/2.74

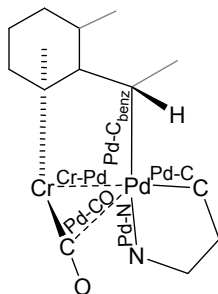[a] associated atom numbering in Figure 3; [b] basis set: *ad hoc* ZORA all electron TZP.

Figure 4 Definition of the geometric parameters listed in Tables 1 and 2.

The most critical distances around the Pd(II) centers (Figure 4) match reasonably well the experimental values determined by X-ray diffraction analysis (Table 1). The dispersion corrected hybrid PBE0 and the metaGGA TPSS

functionals produce Pd-Cr distances by ca. 0.15 Å shorter than in the XRD structures as previously observed.[13-15, 21] It must be noted that dispersion-devoid (ZORA) PBE/all electron TZP level of theory produced significant discrepancies with the X-ray diffraction data that can be related to unaccounted non-local attractive interactions.[21] For a model of **1c**, computed distances Cr-Pd, Pd-Cbenz, Pd-C and Pd-N where found to be longer than in the experimental structure by 0.05, 0.02, 0.02 and 0.04 Å.

The singlet ground state DFT-D geometries all displayed Pd-CO distances by only ca 0.1 Å shorter than in the X-ray diffraction structure. It will be shown thereafter that this shortening does not bias the Pd-CO interaction sufficiently to lead to a bonding donor-acceptor interaction, though. Furthermore, it is shown below that the slightly shorter distances arising form computation do not lead to an overwelming exageration of the role of covalent interactions.

Computational analysis. The relatively low values of the Cr-Pd Wiberg indices, ca. 0.10, immediately argue against a strong contribution of covalence in any of the three compounds. Such magnitudes of Wiberg indices are usually attributed to non-covalent van der Waals interactions between elements. The Pd-C$_{benz}$ bonds show Wiberg indices of ~0.35-~0.37.

While the Wiberg indices are used sparingly as mere indications of the bond order further analysis by Bader's Quantum Theory of Atoms in Molecules (QTAIM) was performed to provide more clarity to the nature of these interactions. To further characterize the interaction between Cr-Pd segments as a result of noncovalent interactions, in all three complexes absence of bond critical point (BCP) was observed. As outlined in Bader's QTAIM conditions for bonding, a bond critical point must be observed along the atomic interaction line or bond path between centers for significant covalent contribution to be considered. However, in all three complexes interactions between the closest carbonyl ligand carbon atom of the Cr(CO)$_3$ fragment with the palladium center were observed to have a BCP(3,-1). The values of interest at the BCPs, ρ (electron density) and its Laplacian $-\frac{1}{4}\nabla^2\rho$, are listed in Table 2 along with the other relevant Pd-X BCPs of complexes **1c** and **3c**. Relatively small values of $-\frac{1}{4}\nabla^2\rho$ at bond critical points between the Pd and Cr(CO)$_3$ carbonyl carbons characterize weak close shell interactions. [44]

Dalton Transactions

ARTICLE

Table 2. QTAIM analysis of bond critical points (3,-1) in complexes **1c** and **3c** with the hybrid (ZORA) PBE0-dDsC / all electron TZP level of theory

1c	ρ (au)	$-\frac{1}{4}\nabla^2\rho$ (au)
Pd -C$_{benz}$	0.098	-0.0435
Pd -C	0.131	-0.0474
Pd -N	0.083	-0.0822
Pd-CO	0.041	-0.0243
Pd-CO	0.035	-0.0185
3c	ρ (au)	$-\frac{1}{4}\nabla^2\rho$ (au)
Pd -C$_{benz}$	0.109	-0.0472
Pd -C	0.125	-0.0382
Pd -N	0.091	-0.0994
Pd-CO	0.047	-0.0276

Yang's noncovalent interaction (NCI) region analysis[35, 36] is also supplied for complexes **1c** and **3c** (see Figure 5); because of the similarity of results between **1c** and **2c** the graphs of the latter have been omitted from consideration. NCI plots are computed on the basis of a threshold value *s* which is determined by contributions of the hessian matrix for the system. This threshold represents the value at which interactions are considered noncovalent or covalent and is inherent to the system. Red-colored regions in the isosurface plot are representative of attractive non-covalent interactions while denoted blue regions are said to be non-bonded or repulsive (Pauli) interactions. In the NCI plots (Figure 5) there is a build up of attractive isosurface for all three structures in the space between the two metals as well as between the chromium and the aromatic carbons, showing the contribution of attractive NCI between the Pd-Cr segment and Cr-aromatic segment. The noted blue interactions shown are primarily in the spaces around the carbonyl structures protruding from the chromium center. Also to be noted are the outer blue regions which are typically depicting the Pauli repulsion interactions arising from steric repulsion. The absence of any strong Pd-CO interaction is clearly discernable from the lack of so-called "covalent throughs"[15] within the attractive NCI isosurfaces separating the carbonyl's carbons and the Pd center.
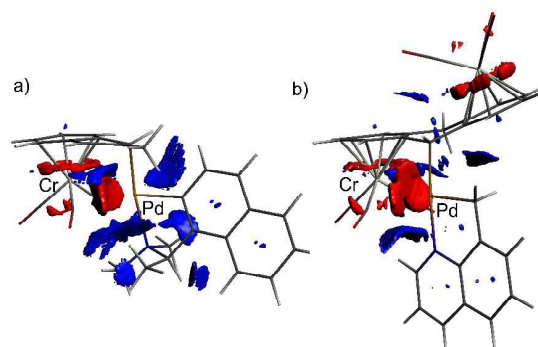

Figure 5 ADFview2013 plots of non-covalent interaction (NCI) regions materialized by reduced density gradient isosurfaces (cut-off value *s*= 0.02 a.u., ρ=0.05 a.u.) colored according to the sign of the signed density $\lambda_2\rho$ (red and blue colors are associated to negatively and positively signed terms) for a gas-phase relaxed singlet ground state model of **1c** (a) and **3c** (b). Calculations were performed with the gas phase singlet ground state geometry optimized at the ZORA-PBE0- dDsC /all electron TZP level.

Yielding additional perspective, NBO[45, 46] analysis was performed to provide insight in the form of orbital interactions as opposed to afore mentioned electron density scheme of QTAIM. It is important to note that the mechanism in which NBO uses to operate will omit any Lewis hybridization states that do not reach the minimum electron occupancy of 1.5 electron.[45, 46] Thus NBO analysis will be presented in the knowledge that highly diffuse interactions, common in bulky transition metal complexes, are not handled completely due to the preset NBO threshold occupancy. NBO was unable to resolve any information about the Cr(CO)$_3$ fragment orbital interactions with the palladium center in all three complexes. Of particular significance is the orbital effect caused by a 3-center interaction observed in the case of complex **3c**. This 3-center interaction, between the ipso aromatic carbon, its immediate benzylic carbon neighbour and the Pd center, had an occupancy of 1.95 electrons and hybrid nature written in the form of a linear combination of natural atomic orbitals

$$\psi_{3\text{-center}}=0.817(sp^{10.5})_{C_{Ar}}+0.490(sp^{49.4}d^{0.02})_{C_{benz}}+0.303(sp^0d^{0.1})_{Pd},$$

which suggests that the palladium center not only interacts with the benzylic position but also with the adjacent ipso aromatic one. This peculiar 3-center interaction can be seen as a consequence of the non-planarity of the hydroanthacenyl unit and of a slightly enhanced delocalisation of the *p* orbital at the benzylic carbon towards the Cr-bound arene, a situation that is not encountered in the NBO analysis of **1c**.

Journal Name

ARTICLE

$$\Delta E_{int} = \Delta E_{Pauli} + \Delta E_{orb} + \Delta E_{el} + \Delta E_{disp}$$

$$\Delta\Delta E_i(X) = \Delta E_i(X) - \Delta E_i(H)$$

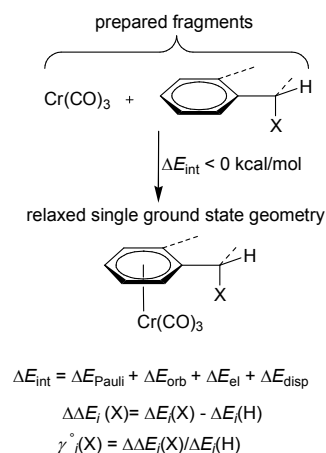$$\gamma^{\circ}{}_i(X) = \Delta\Delta E_i(X)/\Delta E_i(H)$$

Figure 6. Fragmentation scheme used in the energy decomposition analysis (EDA) with the definition of the parameters used in the comparative study of interaction energy terms.

Ziegler–Rauk Energy Decomposition Analysis[47] (EDA) allows the fine partitioning of physical interactions between two arbitrarily chosen so-called prepared fragments; i.e the interaction energy ΔE_{int} that can be partitioned formally into Pauli repulsion ΔE_{Pauli}, orbital ΔE_{orb}, dispersion ΔE_{disp} and electrostatic ΔE_{el} attractive interactions. EDA was used here to analyze the bonding interaction between the $Cr(CO)_3$ moiety and the arene ligand in **1c** and **3c** in order to evaluate the bonding contribution caused by the interaction with the palladacycle. To make the analysis more explicit this effort was also applied to **1a** and **3a**, used here as reference cases for which no major direct interaction exists between the benzylic hydrogens and the $Cr(CO)_3$ moiety. We defined two other parameters $\Delta\Delta E$ and γ° to characterize the variations of arene - $Cr(CO)_3$ interaction energy terms upon replacement of the endo-H (X= H, Figure 6) atom by a palladacycle (X= palladacycle, Figure 6) in singlet ground state geometries; for **1c** and **3c**, X (Figure 6) stands for the pallacyclic units. $\Delta\Delta E$ gives the absolute variation in energy when going say from **1a** (X= H, Figure 6) to **1c** (X=palladacycle, Figure 6) and γ° gives the fraction of variation of either of the interaction energy terms with respect to a reference value (X=H, Figure 6).

Table 3. List of $\Delta\Delta E$ values (in kcal/mol) and associated γ° values (unitless) deduced from EDA carried out at the ZORA-PBE-D3(BJ)/all electron QZ4P level on **1a**, **3a**, **1c** and **3c**.

cmpd	$\Delta\Delta E_{int}$	$\Delta\Delta E_{Pauli}(\gamma^{\circ})$	$\Delta\Delta E_{orb}(\gamma^{\circ})$	$\Delta\Delta E_{disp}(\gamma^{\circ})$	$\Delta\Delta E_{el}(\gamma^{\circ})$
1c	-28	+49(0.31)	-25(0.20)	-6(1.00)	-46(0.46)
3c	-23	+78(0.48)	-34(0.26)	-5(0.84)	-62(0.62)

Table 3 displays the main values obtained for **1c** and **3c**. The first conclusion that can be drawn from these data is

that in hemichelates the Pauli repulsion term arising from the proximity of the palladacycles to the $Cr(CO)_3$ moiety is largely compensated by the sum of orbital, electrostatic and dispersion terms. The strongest attractive term in both cases is the electrostatic, which increases by about 2 times more than the orbital (cf γ° values in brackets, Table 3). The γ° value for the electrostatic term is higher for **3c** and suggests that attractive electrostatic interactions increase by 62 % in **3c** with respect to **3a**, whereas orbital interactions do increase also by only 26 % (vs. 20% in **1c**). This observation supports our continuous claim that attractive electrostatics dominate the stabilization of Pd(II) hemichelates.
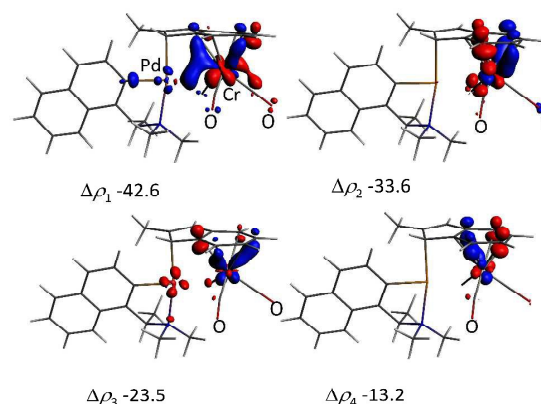

Figure 7. Selected ETS-NOCV deformation densities $\Delta\rho$ and the associated orbital interaction energy ΔE_{orb} (in kcal/mol) for the interaction of closed-shell prepared $Cr(CO)_3$ moieties and the palladated indenyl fragment of **1c** in a singlet ground state gas phase geometry optimized at the ZORA-PBE-D3(BJ)/all electron TZP level. Red and blue-colored isosurfaces materialize regions where charge density depletion and build up occur respectively: electron density transfer operates from red-coloured areas to blue ones upon interaction. Deformation density isosurface contour was set to 0.005 e/bohr³.

The interfragment interaction scheme chosen in the EDA study was used to analyze the orbital interaction component using the ETS-NOCV method. ETS-NOCV is a method for describing the electron deformation density behavior and providing an energetic profile of the orbital interaction between defined interacting fragments. The four highest deformation densities (cf. $\Delta\rho_{1-4}$, Figures 7 and 8) were selected as contributing most significantly to the total orbital interaction energy and are displayed in Figure 7 (**1c**) and Figure 8 (**3c**). In the arene-$Cr(CO)_3$ interaction the greatest part of the interfragment orbital interaction energy arises from establishing the Cr-arene bonds. However, the more "energetic" orbital interaction giving rise to deformation density isosurface $\Delta\rho_1$ (Figure 6 and 7) includes a residual direct charge density buildup towards the Pd center, which in the case of **1c** and **3c** essentially originates from the Cr. In both complexes this Cr-to-Pd donation entails electron density transfer from orbitals

Dalton Transactions

ARTICLE

located at the Cr center toward the intermetallic space and orbitals localed at the Pd. In **1c**, $\Delta\rho_2$ and $\Delta\rho_3$ materialize the backdonation of the Pd mostly to Cr-arene bonds. In **3c**, $\Delta\rho_3$ materializes the strongest back-donation of the Pd center towards Cr-arene bonds.
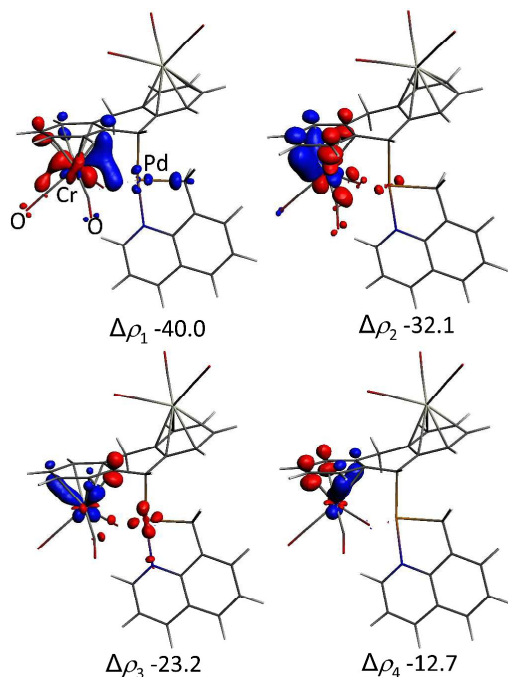

Figure 8 Selected ETS-NOCV deformation densities $\Delta\rho$ and the associated orbital interaction energy ΔE_{orb} (in kcal/mol) for the interaction of closed-shell prepared $Cr(CO)_3$ moieties and the palladated 9-hydroanthracenyl fragment of **3c** in a singlet ground state gas phase geometry optimized at the ZORA-PBE-D3(BJ)/all electron TZP level. Red and blue-colored isosurfaces materialize regions where charge density depletion and build up occur respectively: electron density transfer operates from red-coloured areas to blue ones upon interaction. Deformation density isosurface contour was set to 0.005 e/bohr³.

Conclusions

The results disclosed herein clearly suggest that the establishment of a Cr-C(O)…Pd interaction is in no way a prerequisite for the non-covalent stabilization of the unsaturated palladium center. At present it is difficult to accurately define quantitatively the nature of the interaction between the two metal moieties and particularly the contribution of covalence, i.e charge transfer (orbital interactions), which QTAIM and NCI analyses only qualitatively characterize as non-dominating. Comparative EDA analysis using **1a** and **3a** as reference cases provides a rough estimate of the enhancement of the orbital interaction energy term in **1c** and **3c**, the increase of

which is much less than that of the electrostatic term. The enhancement of the electrostatic term can be related to the proximity of the electron deficient Pd centre positionned close by the electron rich $Cr(CO)_3$ moiety. It is speculated that any increase of the covalent character of the $[Cr(CO)_3]$-M interaction would result in the oxidation of the Cr^0 center and the reduction of the M center thus leading to the formation of paramagnetic species, the stability of which is hardly predictable. To date such a situation was not encountered, except perhaps in one recently reported case[15] that gave rise to a new example of stable hemichelate of the Pd(I)-Pd(I) unit; all reported hemichelates display in general diamagnetic behaviour. It is not excluded though that exogenous physical perturbations, like exposure to light, may promote such charge transfer and open access to new chemical properties. Ongoing research is focussing on the chemical properties and reactivity of hemichelates, the results of which will be disclosed in due time.

Experimental

General. All experiments were carried out under a dry argon atmosphere using standard Schlenk techniques or in an argon-filled glove-box when necessary. *n*-Butyllithium was purchased from Aldrich Chem. Co as a 1.6 M solution in hexanes, hexacarbonylchromium was purchased from ABCR, 9,10-dihydroanthracene (99 %) was purchased from Aldrich Chem. Co and 1,2-di(3-indenyl)ethane (98 %) from Alfa Aesar. Complexes **1a**,[21] **1b**,[48] **2b**,[49] **3a**[50] and **3b**[51] were prepared according to published synthetic procedures. Celite 545 was purchased from VWR Prolabo. Anhydrous tetrahydrofurane (abbr. THF) and diethylether were distilled from purple solutions of Na/benzophenone under argon. All other solvents were distilled over sodium or CaH_2 under argon. Deuterated solvents were dried over sodium or CaH_2 and purified by trap-to-trap techniques, degassed by freeze-pump-thaw cycles and stored under argon. ^1H, ^{13}C NMR spectra were obtained on Bruker DPX 300, 400, Avance I 500 and Avance III 600 spectrometers. Chemical shifts (expressed in parts per million) were referenced against solvent peaks. Full NMR spectral assignments are provided in the Electronic Supporting Information; the atomic numbering scheme used for NMR assignments is detailed below. Infrared spectra of powdered amorphous samples were acquired with a Fourier transform-IR Bruker Alpha spectrometer using an ATR solid state sample cell. The circular dichroism spectrum of **1c** in solution was recorded with a UV-visible JASCO J-810 spectropolarimeter using a 20°C Peltier-thermostated quartz cell of 1 cm optical path.

Crystal structure resolution. Acquisition and processing parameters are displayed in Table 4. Reflections were

Journal Name

ARTICLE

collected with Nonius KappaCCD and APEX diffractometers equipped with an Oxford Cryosystem liquid N_2 device, using Mo-Kα radiation (λ = 0.71073 Å). The crystal-detector distance was 38 mm. The cell parameters were determined (APEX2 software[52]) from reflections taken from three sets of 12 frames, each at 10 s exposure. The structures were solved by direct methods using the program SHELXS-97.[53] The refinement and all further calculations were carried out using SHELXL-97.[54] The crystal structures acquired with the Nonius Kappa CCD were solved using SIR-97[55] and refined with SHELXL-97.[54] The refinement and all further calculations were carried out using SHELXL-97.[54] The H-atoms were included in calculated positions and treated as riding atoms using SHELXL default parameters. The non-H atoms were refined anisotropically, using weighted full-matrix least-squares on F^2. A semi-empirical absorption correction was applied using SADABS in APEX2.[52]

Computational details. Computations were performed with methods of Density Functional Theory, i.e the PBE[56] GGA, the meta-GGA TPSS[57] and the hybrid PBE0[58, 59] functionals implemented in the Amsterdam Density Functional package (ADF2013[40] version) and augmented with Grimme's DFT-D3(BJ)[60, 61] implementation of dispersion with a Becke-Johnson (BJ) damping function (PBE-D3(BJ)

and TPSS-D3(BJ)) and with Corminboeuf's DdSc[62] density dependent dispersion correction (PBE0-DdSc). Scalar relativistic corrections with the Zeroth Order Regular Approximation[63-65] were applied with ad hoc all-electron (AE) basis sets consisting of polarized triple-ζ (TZP) Slater type orbitals. Geometry optimization by energy gradient minimization was carried out in all cases with a numerical grid accuracy comprised between 4.5 and 8, an energy gradient convergence criterion of 10^{-3} au and a very tight SCF convergence criterion. Vibrational modes were computed to verify that the optimized geometries were related to energy minima not considering residual modes comprised between 0 and 50 $i$cm^{-1}. AIM,[44, 66] NCI,[35, 36] ETS-NOCV,[32, 33] NBO[46] (GENNBO v.6) and EDA[47] analyses were carried out using the modules embedded within ADF2013. EDA analyses were performed at the PBE-D3(BJ)/all electron QZ4P level on geometries optimized at the PBE-D3(BJ)/all electron TZP level. CD response of **1c** was computed using the SAOP[37, 38] potential combined with an all electron ZORA-devised TZ2P basis set for all elements. Representations of molecular structures and isosurfaces were produced with ADFview 2013.

Dalton Transactions

Table 4. List of acquisition and refinement data for the structural X-ray diffraction analyses of compounds **1c-3c**.

	1c	2c	3c
formula	$C_{27}H_{25}CrNO_3Pd$	$C_{44}H_{40}Cr_2N_2O_6Pd_2$	$C_{30}H_{19}Cr_2NO_6Pd$
mol. wt	569.88	1009.58	699.86
cryst. syst.	monoclinic	triclinic	monoclinic
space group	$P2_1$	$P\bar{1}$	$P2_1/c$
T (K)	150	173	173
a (Å)	10.346(1)	7.6062(4)	9.0689(10)
b (Å)	10.356(1)	9.3530(5)	20.282(3)
c (Å)	10.670(1)	17.0014(9)	14.2127(16)
α (°)		103.793(1)	
β (°)	90.978(1)	100.439(1)	105.006(7)
γ (°)		98.617(1)	
V (Å^3)	1143.05(19)	1131.33(10)	2525.1(5)
Z	2	1	4
μ (mm^{-1})	1.29	1.30	1.60
cryst. size (mm)	0.26×0.22×0.06	0.20×0.18×0.15	0.20×0.15×0.10
T_{min}, T_{max}	0.730, 0.927	0.659, 0.746	0.710, 0.960
no. measd rflns	8366	18570	12666
no. indept rflns	5580	6588	5510
no. obsd [$I > 2\sigma(I)$] rflns	5430	5240	2477
R_{int}	0.027	0.030	0.097
$R[F^2 > 2\sigma(F^2)]$	0.029	0.033	0.075
$wR(F^2)$	0.071	0.078	0.224
S	1.00	1.02	1.03
no. params	373	255	361
$\Delta\rangle_{max}$, $\Delta\rangle_{min}$ (e Å^{-3})	0.44, -0.51	0.96, -0.49	1.16, −1.02
Flack param.	0.02 (3)	–	-

Synthesis of 1c. **1a** (0.200 g, 0.75 mmol) was dissolved in THF (5 mL) and treated with *n*-BuLi (0.52 mL, 0.83 mmol) at -40 °C under argon. The resulting solution was transferred after 30 min *via* canula to another Schlenk vessel containing a THF (3 mL) solution of **1b** (0.261 g, 0.38 mmol). The resulting solution was stirred for 1 hour and temperature was slowly raised to -5 °C. At this temperature, the solvent was removed under reduced pressure. The residue was then washed with cold diethylether to remove soluble impurities. Extraction with dichloromethane was performed, followed by a filtration through celite and recrystallization from a dichloromethane/pentane mixture of solvents, which led to **1c** as an orange solid (0.313 g, 73 %). Calcd for $C_{27}H_{25}CrNO_3Pd$: C, 56.90; H, 4.42; N, 2.46. Found: C, 56.77; H, 4.41; N, 2.29. HRMS-ESI (*m/z*): $[M+Na]^+$ calcd for $C_{27}H_{25}CrNO_3Pd$, 592.0167; found, 592.0236. IR (cm^{-1}) ν(CO): 1935 (s), 1865 (s), 1843 (vs). $[\alpha]_D$ (298 K)= -267.3 (*c* 0.052, 298.15 K, benzene). CD (benzene, 293 K) λ_{max} (Mol. Ellip.) 305 (-5494), 312 (-10368), 322 (-3091), 338 (-11253), 366 (-7094), 413 (-17765), 470 (3442), 530 (-384). ^{1}H NMR (500 MHz, C$_6$D$_6$, 293 K) δ 8.06 (d, J = 8.3 Hz, 1H, H$_{13}$), 7.82 (d, J = 7.6 Hz, 1H, H$_{16}$), 7.70 (d, J = 8.5 Hz, 1H, H$_{14}$), 7.58 (d, J = 7.6 Hz, 1H, H$_{19}$), 7.37 − 7.30 (m,

2H, H$_{17}$, H$_{18}$), 5.62 (s, 1H, H$_3$), 5.27 (d, J = 6.4 Hz, 1H, H$_4$), 5.17 (d, J = 6.7 Hz, 1H, H$_7$), 4.98 (td, J = 6.5, 0.9 Hz, 1H, H$_6$), 4.44 (s, 1H, H$_1$), 4.08 (td, J = 6.4, 1.1 Hz, 1H, H$_5$), 3.80 (q, J = 6.4 Hz, 1H, H$_{22}$), 2.54 (s, 3H, H$_{24}$), 2.45 (s, 3H, H$_{25}$), 2.03 (s, 3H, H$_8$), 1.72 (d, J = 6.4 Hz, 3H, H$_{23}$). ^{13}C NMR (126 MHz, C$_6$D$_6$, 293 K) δ 239.53 (bs, C$_{11}$), 237.3 (bs, C$_{10}$), 235.2 (bs, C$_9$), 161.8 (C$_2$), 157.0 (C$_{12}$), 148.5 (C$_{21}$), 132.7 (C$_{13}$), 132.4 (C$_{15}$), 130.1 (C$_{20}$), 129.4 (C$_{16}$), 125.9 (C$_{17}$), 125.5 (C$_{14}$), 124.1 (C$_{18}$), 124.1 (C$_{19}$), 115.9 (C$_{7'}$), 111.5 (C$_3$), 108.0 (C$_{3'}$), 95.0 (C$_4$), 93.8 (C$_6$), 90.2 (C$_7$), 87.7 (C$_5$), 74.4 (C$_{22}$), 51.5 (C$_{24}$), 51.2 (C$_1$), 48.2 (C$_{25}$), 22.3 (C$_{23}$), 17.7 (C$_8$) (cf. Figure 9).
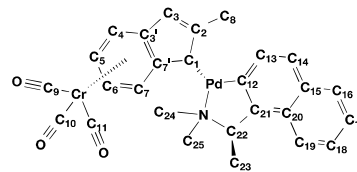
Figure 9 Atomic numbering scheme for the assignment of ^{1}H and ^{13}C NMR signals in **1c**.

Journal Name

ARTICLE

Synthesis of 2a. $Cr(CO)_6$ (11.499 g, 52.25 mmol), 1,2-bis(3-indenyl)ethane (5.0 g, 19.35 mmol), naphthalene (0.335 g, 2.61 mmol), THF (15 mL), and di-$n$butylether (150 mL) were gently refluxed for 135 h under a permanent flow of argon. The resulting orange/red solution was evaporated to dryness and the resulting residue was adsorbed on silica gel. Chromatographic separation was performed on silica gel using a mixture of CH_2Cl_2 and pentane (1:1 to 1:0) as eluent. **2a** was eluted as an orange-coloured solution containing isomers A and B, namely **A-2a** and **B-2a** the respective spectroscopic signatures of which were characterized a posteriori. Removal of the solvents under reduced pressure afforded an orange solid (1.57 g, 19.3 mmol, 15 %). Calcd for $C_{26}H_{18}Cr_2O_6$: C, 58.88; H, 3.42. Found: C, 59.10; H, 3.75. HRMS-ESI (m/z): $[M+1Na]^+$ calcd for $C_{26}H_{18}Cr_2O_6$, 552.9806; found, 552.9810. IR (cm^{-1}) ν(CO): 1940 (s), 1840 (vs). Isomer **A-2a**: ^{1}H NMR (500 MHz, C_6D_6, 293 K) δ 5.69 (bd, J = 26.2 Hz, 4H, H_2, H_{13}), 5.24 (d, J = 6.2 Hz, 2H, H_5), 4.91 (d, J = 6.2 Hz, 2H, H_8), 4.53 – 4.45 (m, 2H, H_7, H_{17}), 4.45 – 4.36 (m, 2H, H_6, H_{18}), 2.90 (dd, J = 23.0, 7.3 Hz, 1H, H_{1a}, H_{14a}), 2.68 (d, J = 23.0 Hz, 1H, H_{1b}, H_{14b}), 2.52 – 2.38 (m, 2H, H_{10}), 2.37 – 2.27 (m, 2H, H_{11}). ^{13}C NMR (126 MHz, C_6D_6, 293 K) δ 234.3 (C_{22}, C_{21}, C_{23}, C_{25}, C_{24}, C_{26}), 141.2 (C_3, C_{12}), 130.8 (C_2, C_{13}), 114.9 (C_4, C_{20}), 114.5 (C_9, C_{15}), 91.4 (C_7, C_{17}), 90.0 (C_6, C_{18}), 89.8 (C_8, C_{16}), 87.3 (C_5, C_{19}), 37.9 (C_1, C_{14}), 25.1 (C_{10}, C_{11}). Isomer **B-2a**: ^{1}H NMR (500 MHz, C_6D_6, 293 K) δ 5.69 (bd, J = 26.2 Hz, 2H, H_2, H_{13}), 5.01 (d, J = 6.2 Hz, 2H, H_5, H_{19}), 4.95 (d, J = 6.2 Hz, 2H, H_8, H_{16}), 4.53 – 4.45 (m, 2H, H_7, H_{17}), 4.45 – 4.36 (m, 2H, H_6, H_{18}), 2.90 (dd, J = 23.0, 7.3 Hz, 2H, H_{1a}, H_{14a}), 2.68 (d, J = 23.0 Hz, 2H, H_{1b}, H_{14b}), 2.52 – 2.38 (m, 2H, H_{10}), 2.37 – 2.27 (m, 2H, H_{11}). ^{13}C NMR (126 MHz, C_6D_6, 293 K) δ 234.2 (C_{22}, C_{21}, C_{23}, C_{25}, C_{24}, C_{26}), 141.5 (C_3, C_{12}), 130.4 (C_2, C_{13}), 115.2 (C_4, C_{20}), 114.0 (C_9, C_{15}), 90.9 (C_7, C_{17}), 90.3 (C_6, C_{18}), 90.1 (C_8, C_{16}), 86.7 (C_5, C_{19}), 37.9 (C_1, C_{14}), 24.9 (C_{10}, C_{11}) (cf. Figure 10).
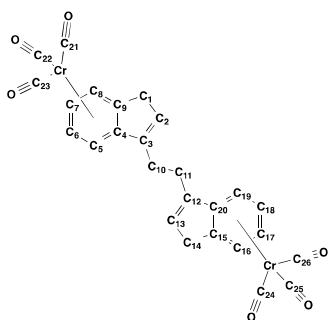

Figure 10. Atomic numbering scheme for the assignment of ^{1}H and ^{13}C NMR signals of **2a**.

Synthesis of 2c. **2a** (0.100 g, 0.19 mmol) was dissolved in THF (5 mL) and treated with n-BuLi (0.26 mL, 0.41 mmol) at -40 °C under argon. The resulting solution was transferred after 30 min

via canula to another Schlenk vessel containing a THF (3 mL) solution of **2b** (0.115 g, 0.21 mmol). The resulting solution was stirred for 1 hour whilst temperature was slowly raised to -5 °C. At this temperature, the solvent was removed under reduced pressure. The residue was then washed with cold diethyl ether to remove soluble impurities. Finally extraction with dichloromethane was performed, followed by a filtration over celite and recrystallization from a dichloromethane/pentane mixture of solvents, which produced 2c as an orange solid (0.033 g, 0.03 mmol, 17 % yield). Calcd for $C_{44}H_{40}Cr_2N_2O_6Pd_2$·1/5$CH_2Cl_2$: C, 51.71; H, 3.97; N, 2.73. Found: C, 51.73; H, 4.10; N, 2.66. HRMS-ESI (m/z): $[M]^+$ calcd for $C_{44}H_{40}Cr_2N_2O_6Pd_2$, 1007.9766; found, 1007.9869. IR (cm^{-1}) ν(CO): 1936 (s), 1875 (s), 1842 (vs). ^{1}H NMR (500 MHz, $CDCl_3$, 293 K) δ 7.63 (d, J = 7.4 Hz, 2H, H_{28}, H_{37}), 7.19 (t, J = 7.3 Hz, 2H, H_{29}, H_{38}), 7.16 (d, J = 6.1 Hz, 2H, H_{31}, H_{40}), 7.11 (t, J = 7.3 Hz, 2H, H_{30}, H_{39}), 6.77 (d, J = 2.1 Hz, 2H, H_2, H_{13}), 6.02 (d, J = 6.7 Hz, 2H, H_5, H_{19}), 5.97 (d, J = 6.4 Hz, 2H, H_8, H_{16}), 5.93 (t, J = 6.2 Hz, 2H, H_6, H_{18}), 5.09 (t, J = 6.4 Hz, 2H, H_7, H_{17}), 4.47 (d, J = 2.1 Hz, 2H, H_1, H_{14}), 3.92 (d, J = 13.1 Hz, 2H, H_{33a}, H_{42a}), 3.64 (d, J = 13.1 Hz, 2H, H_{33b}, H_{42b}), 2.65 (s, 6H, H_{34}, H_{43}), 2.51 (s, 6H, H_{35}, H_{44}), 2.48 (s, 4H, H_{10}, H_{11}). ^{13}C NMR (126 MHz, $CDCl_3$, 293 K) δ 238.7 (bs, C_{23}, C_{26}), 236.4 (bs, C_{22}, C_{25}), 232.7 (bs, C_{21}, C_{24}), 156.5 (C_{27}, C_{36}), 148.0 (C_{32}, C_{41}), 141.3 (C_2, C_{13}), 132.2 (C_{28}, C_{37}), 126.2 (C_{29}, C_{38}), 124.4 (C_{30}, C_{39}), 124.3 (C_3, C_{12}), 123.6 (C_{31}, C_{40}), 116.2 (C_4, C_{20}), 106.4 (C_9, C_{15}), 95.9 (C_8, C_{16}), 94.1 (C_6, C_{18}), 90.3 (C_5, C_{19}), 88.4 (C_7, C_{17}), 73.5 (C_{33}, C_{42}), 51.0 (C_{35}, C_{44}), 50.3 (C_{34}, C_{43}), 46.3 (C_1, C_{14}), 25.9 (C_{10}, C_{11}) (cf. Figure 11).
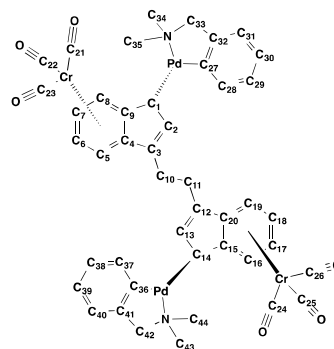

Figure 11. Atomic numbering scheme for the assignment of ^{1}H and ^{13}C NMR signals of **2c**.

Synthesis of 3a. The synthesis of **3a** was performed according to the methods proposed by Bitterwolf and co-workers.[50] A mixture of $Cr(CO)_6$ (9.8 g, 44.4 mmol), 9,10-dihydroanthracene (2.0 g, 11.1 mmol), naphtalene (0.284 g, 2.2 mmol), THF (15 mL), and di-$n$butylether (150 mL) was gently refluxed for 111 h under a permanent flow of argon. The resulting orange/red solution

Dalton Transactions

ARTICLE

was evaporated to dryness and the resulting residue was adsorbed on silica gel. Chromatographic separation was performed on silica gel using a mixture of CH_2Cl_2 and acetone (90:10 to 10:90) as eluent. A band containing the product was eluted as an orange solution, which afforded *trans*-bistricarbonyl[η^6,η^6-(9,10-dihydroanthracene)]chromium(0) as an orange solid upon removal of the solvents under reduced pressure (3.05 g, 6.74 mmol, 61 %). Analytical and spectroscopic data were identical to those reported in the literature.[50]

Synthesis of 3c. A solution of *trans*-bistricarbonyl[η^6,η^6-(9,10-dihydroanthracene)]chromium(0) **3a** (0.200 g, 0.44 mmol) in THF (15 mL) was treated with 1.1 equivalent of *n*-BuLi (0.30 mL, 0.49 mmol) at -40 °C. The resulting solution of anion was transfered after 30 min at -40 °C via a cannula to a THF solution (10 mL) containing 0.7 equivalent of **3b** (0.128 g, 0.23 mmol). The resulting mixture was stirred for 1 h and the temperature was slowly raised to -20 °C. The solvent was concentrated under reduced pressure to produce a highly moisture and air sensitive material that escaped full characterization due to massive decomposition upon repeated attempts of purification by the slow diffusion of the crude reaction mixture into dry n-heptane at -40°C. However, in one attempt minute amounts of orange/red crystals of **3c** were obtained.

Notes and references.

[a] Institut de Chimie de Strasbourg, UMR 7177, Université de Strasbourg, 4 rue Blaise Pascal, F-67000 Strasbourg.
[b] home institution: Northwest Missouri State University
[c] Département de Chimie, Ecole Polytechnique CNRS, Route de Saclay, F-91128 Palaiseau Cedex, France
† Electronic Supplementary Information (ESI) available: NMR spectra of **1c**, **2a**, **2c**, experimental and computed CD spectrum of **1c**, cartesian coordinates, energies and vibrational modes of computed models of **1c**, **2c** and **3c**, CIF deposited with CCDC with reference numbers 1425361-1425363 for compounds **1c-3c** are available. For ESI and crystallographic data in CIF or other electronic format see DOI: 10.1039/b000000x/

1. W. B. Jensen, *J. Chem. Ed.*, 2005, **82**, 28.
2. I. Langmuir, *Science* 1921, **54**, 59-67
3. S. Giri, B. Z. Child, J. Zhou and P. Jena, *RSC Adv.*, 2015, **5**, 44003-44008.
4. M. B. Abreu, A. C. Reber and S. N. Khanna, *J. Phys. Chem. Lett.*, 2014, **5**, 3492-3496.
5. A. D. Brathwaite, J. A. Maner and M. A. Duncan, *Inorg. Chem.*, 2014, **53**, 1166-1169.
6. G. W. Waldhart, A. J. Webster, B. M. Schreiber, R. B. Siedschlag and J. S. D'Acchioli, *J. Inorg. Organomet. Polym. Mater.*, 2014, **24**, 87-94.
7. M. C. Baird, *J. Organomet. Chem.*, 2014, **751**, 50-54.
8. X. Zhang, Q.-s. Li, Y. Xie, R. B. King and H. F. Schaefer, III, *J. Mol. Struct.*, 2008, **890**, 184-191.
9. M. Ahlquist, P. Fristrup, D. Tanner and P.-O. Norrby, *Organometallics*, 2006, **25**, 2066-2073.
10. R. F. W. Bader, *J. Phys. Chem. A*, 2010, **114**, 7431-7444.
11. R. J. Gillespie and E. A. Robinson, *J. Comput. Chem.*, 2007, **28**, 87-97.
12. R. J. Gillespie and B. Silvi, *Coord. Chem. Rev.*, 2002, **233-234**, 53-62.
13. C. Werle, C. Bailly, L. Karmazin-Brelot, X.-F. Le Goff, L. Ricard and J.-P. Djukic, *J. Am. Chem. Soc.*, 2013, **135**, 17839-17852.
14. C. Werle, C. Bailly, L. Karmazin-Brelot, X.-F. Le Goff, M. Pfeffer and J.-P. Djukic, *Angew. Chem., Int. Ed.*, 2014, **53**, 9827-9831.
15. C. Werlé, L. Karmazin, C. Bailly, L. Ricard and J.-P. Djukic, *Organometallics*, 2015, **34**, 3055-3064.
16. P. Petrović, J.-P. Djukic, A. Hansen, C. Bannwarth and S. Grimme, in *Non-covalent Interactions in Synthesis and Design of New Compounds*, eds. A. M. Maharramov, K. T. Mahmudov, M. N. Kopylovich and A. J. L. Pombeiro, John Wiley & Sons, Inc., Hoboken, New Jersey, 2016, p. in press.
17. J.-P. Djukic, M. Pfeffer and K. H. Dotz, *C. R. Acad. Sci., Ser. IIc: Chim.*, 1999, **2**, 403-408.
18. J.-P. Djukic, A. Maisse-Francois, M. Pfeffer, K. H. Doetz, A. De Cian and J. Fischer, *Organometallics*, 2000, **19**, 5484-5499.
19. J.-P. Djukic, C. Michon, A. Maisse-Francois, R. Allagapen, M. Pfeffer, K. H. Dotz, A. De Cian and J. Fischer, *Chem. Eur. J.*, 2000, **6**, 1064-1077.
20. J.-P. Djukic, A. Maisse, M. Pfeffer, K.-H. Doetz and M. Nieger, *Eur. J. Inorg. Chem.*, 1998, 1781-1790.
21. C. Werle, M. Hamdaoui, C. Bailly, X.-F. Le Goff, L. Brelot and J.-P. Djukic, *J. Am. Chem. Soc.*, 2013, **135**, 1715-1718.
22. C. Werle, X.-F. Le Goff and J.-P. Djukic, *J. Organomet. Chem.*, 2014, **751**, 754-759.
23. R. B. King, *Inorg. Chim. Acta*, 2003, **350**, 126-130.
24. R. Colton and M. J. McCormick, *Coord. Chem. Rev.*, 1980, **31**, 1-52.

Journal Name

ARTICLE

25. W. I. Dzik, C. Creusen, R. de Gelder, T. P. J. Peters, J. M. M. Smits and B. de Bruin, *Organometallics*, 2010, **29**, 1629-1641.

26. R. D. Adams, Z. Li, J. C. Lii and W. Wu, *J. Am. Chem. Soc.*, 1992, **114**, 4918-4920.

27. T. E. Wolff and L. P. Klemann, *Organometallics*, 1982, **1**, 1667-1670.

28. I. A. Oxton, *J. Mol. Struct.*, 1982, **78**, 77-84.

29. M. Cowie and S. K. Dwight, *Inorg. Chem.*, 1980, **19**, 2508-2513.

30. P. Macchi, L. Garlaschelli and A. Sironi, *J. Am. Chem. Soc.*, 2002, **124**, 14173-14184.

31. P. Macchi and A. Sironi, *Coord. Chem. Rev.*, 2003, **238-239**, 383-412.

32. M. P. Mitoraj, A. Michalak and T. Ziegler, *J. Chem. Theory Comput.*, 2009, **5**, 962-975.

33. M. P. Mitoraj, A. Michalak and T. Ziegler, *Organometallics*, 2009, **28**, 3727-3733.

34. J. Moellmann and S. Grimme, *Organometallics*, 2013, **32**, 3784-3787.

35. J. Contreras-Garcia, E. R. Johnson, S. Keinan, R. Chaudret, J. P. Piquemal, D. N. Beratan and W. Yang, *J. Chem. Theor. Comput.*, 2011, **7**, 625-632.

36. E. Johnson, S. Keinan, P. Mauri-Sanchez, J. Contreras-Garcia, A. J. Cohen and W. Yang, *J. Am. Chem. Soc.*, 2010, **132**, 6498-6506.

37. O. V. Gritsenko, P. R. T. Schipper and E. J. Baerends, *Chem. Phys. Lett.*, 1999, **302**, 199-207.

38. P. R. T. Schipper, O. V. Gritsenko, S. J. A. van Gisbergen and E. J. Baerends, *J. Chem. Phys.*, 2000, **112**, 1344-1352.

39. G. te Velde, F. M. Bickelhaupt, E. J. Baerends, C. Fonseca Guerra, S. J. A. van Gisbergen, J. G. Snijders and T. Ziegler, *J. Comp. Chem.*, 2001, **22**, 931-967.

40. Amsterdam Density Functional ADF2013, SCM, Theoretical Chemistry, Vrije Universiteit, Amsterdam, The Netherlands, 2013.

41. S. Grimme and J.-P. Djukic, *Inorg. Chem.*, 2011, **50**, 2619-2628.

42. T. Schwabe, S. Grimme and J. P. Djukic, *J. Am. Chem. Soc.*, 2009, **131**, 14156-14157.

43. S. Grimme and J.-P. Djukic, *Inorg. Chem.*, 2010, **49**, 2911-2919.

44. P. Popelier, *Atoms in Molecules, An Introduction*, Prentice Hall, Harlow, England, 2000.

45. F. Weinhold and C. R. Landis, *Valency and Bonding, a natural bond orbital donor-acceptor perspective*, University Press, Cambridge, UK, 2005.

46. F. Weinhold, in *Encyclopedia of Computational Chemistry*, eds. P. vonRagué-Schleyer, N. L. Allinger, T. Clark, J. Gasteiger, P. A. Kollman, H. F. Schaefer and P. R. Schreiner, John Wiley & Sons, Chichester, UK, 1998, vol. 3, pp. 1792-1811.

47. T. Ziegler and A. Rauk, *Inorg. Chem.*, 1979, **18**, 1755-1759.

48. D. G. Allen, G. M. McLaughlin, G. B. Robertson, W. L. Steffen, G. Salem and S. B. Wild, *Inorg. Chem.*, 1982, **21**, 1007-1014.

49. A. C. Cope and E. C. Friedrich, *J. Am. Chem. Soc.*, 1968, **90**, 909-913.

50. T. E. Bitterwolf, R. Herzog and P. D. Rockswold, *J. Organomet. Chem.*, 1987, **320**, 197-209.

51. G. E. Hartwell, R. V. Lawrence and M. J. Smas, *J. Chem. Soc. D*, 1970, 912.

52. M86-E01078 APEX2 User Manual, Bruker AXS Inc., Madison, USA, 2006.

53. G. M. Sheldrick, *Acta Crystallogr., Sect. B*, 1990, **A46**, 467-473.

54. M. Sheldrick, Göttingen, Germany, 1998.

55. A. Altomare, M. C. Burla, M. Camalli, G. Cascarano, C. Giacovazzo, A. Guagliardi, A. G. G. Moliterni, G. Polidori and R. Spagna, SIR97, an integrated package of computer programs for the solution and refinement of crystal structures using single-crystal data, 1999.

56. J. P. Perdew, K. Burke and M. Ernzerhof, *Phys. Rev. Lett.*, 1996, **77**, 3865-3868.

57. J. Tao, J. P. Perdew, V. N. Staroverov and G. E. Scuseria, *Phys. Rev. Lett.*, 2003, **91**, 146401.

58. M. Ernzerhof and G. E. Scuseria, *J. Chem. Phys.*, 1999, **110**, 5029-5036.

59. C. Adamo and V. Barone, *J. Chem. Phys.*, 1999, **110**, 6158.

60. S. Grimme, S. Ehrlich and L. Goerigk, *J. Comp. Chem.*, 2011, **32**, 1456-1465.

61. S. Grimme, *Wiley Interdisciplinary Reviews: Computational Molecular Science*, 2011, **1**, 211-228.

62. S. N. Steinmann and C. Corminboeuf, *J Chem. Theor. Comp.*, 2011, **7**, 3567-3577.

63. E. van Lenthe, E. J. Baerends and J. G. Snijders, *J. Chem. Phys.*, 1993, **99**, 4597-4610.

64. E. van Lenthe, E. J. Baerends and J. G. Snijders, *J. Chem. Phys.*, 1994, **101**, 9783-9792.

65. E. van Lenthe, A. Ehlers and E.-J. Baerends, *J. Chem. Phys.*, 1999, **110**, 8943-8953.

66. R. F. W. Bader, in *Atoms in Molecules: A Quantum Theory*, Clarendon, Oxford, 1990, ch. 7.

Three novel *hemichelates* of Pd(II) resulting from reaction of indene and hydrophenanthrene-based organometallic anions with three µ-chloro-bridged palladacycles are reported.
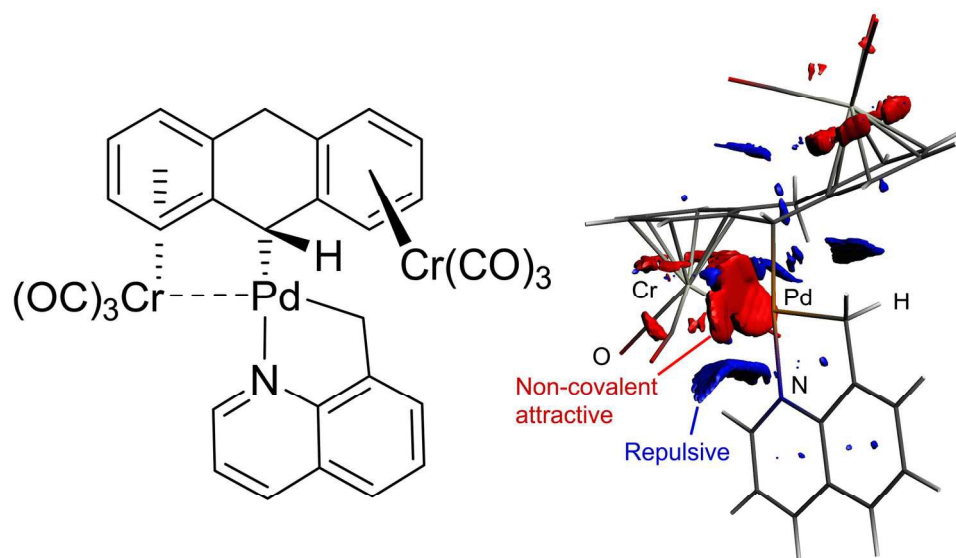
Table of content graphic
156x93mm (300 x 300 DPI)